Removal of antibiotics from black water by a membrane filtration-visible light photocatalytic system

Hongbo Liu, Haodong Zhang, Xinyi Dong, Chengyang Wu, Eric Lichtfouse

Journal of Water Process Engineering 53 (2023) 103605

https://doi.org/10.1016/j.jwpe.2023.103605

Removal of antibiotics from black water by a membrane filtration-visible light photocatalytic system

Hongbo Liu [a,*], Haodong Zhang [a], Xinyi Dong [a], Chengyang Wu [a], Eric Lichtfouse [b]

[a] School of Environment and Architecture, University of Shanghai for Science and Technology, 516 Jungong Road, 200093 Shanghai, China
[b] Aix-Marseille Univ, CNRS, IRD, INRA, Coll France, CEREGE, 13100 Aix en Provence, France

ARTICLE INFO

Keywords:
Black water
Filtration-photocatalytic membrane
g-C_3N_4/TiO_2
Sulfamethoxazole
Tetracycline

ABSTRACT

To address the problem of pollution caused by antibiotics in black water, we synthesized membranes containing the g-C_3N_4/TiO_2 photocatalysts and tested them for the removal of sulfamethoxazole (SMZ) and tetracycline (TC) in pure water conditions and black water. We compared the basic membrane filtration and photocatalytic performance of the g-C_3N_4/TiO_2 and the PVDF membranes, and investigated the influencing factors and application aspects of membrane filtration-photocatalytic systems for antibiotic removal. The anti-fouling performance and re-usability of g-C_3N_4/TiO_2 membranes were investigated by evaluating the fouling reversibility of photocatalytic membranes. The results showed that g-C_3N_4/TiO_2 improved the porosity, hydrophilicity and permeability of the membranes significantly. PgT-3 (PVDF/g-C_3N_4/TiO_2) membrane with 0.03 wt% of g-C_3N_4/TiO_2 has the best overall performance with 72.8 % and 63.9 % removal efficiency for SMZ and TC respectively. Neutral or weakly acidic solution (pH = 5.0–7.0) is favorable for the removal of both study antibiotics. The complex composition of black water increased the adsorption load on the membrane and caused the inhibition of the photocatalysis of the g-C_3N_4/TiO_2 membrane. The absorption of visible light by g-C_3N_4 accelerates the electron transfer rate and promotes the separation of electrons from holes. The oxidation-active substance h^+ produced in the system plays an important role in the removal of SMZ and TC.

1. Introduction

With the continuous development of the pharmaceutical industry, antibiotics have been developed and used for their high potency and broad spectrum, oral activity, and other advantages [1,2]. Currently, there are thousands of antibiotic species produced, which are widely used in the fields of medical treatment, livestock and poultry breeding, aquaculture, etc. The antibiotics commonly used in human medical treatment include five major categories: sulfonamides, tetracyclines, fluoroquinolones, macrolides, and β-lactams [3]. Studies show that about 58.2 % of the antibiotics currently used are discharged directly into the natural environment in their parent forms and enter the natural cycle through feces, posing a great threat to the ecological environment [4]. The continuous accumulation of antibiotics in the natural environment can pose a series of adverse effects on the environment, plants and animals, and human health [5], such as leading to the development of bacterial resistance and interference with human endocrine [6,7].

China is the largest user of antibiotics and a substantial source of antibiotics was released into the environment via human feces [8]. The existing investigations focus on antibiotics in drinking water, livestock manure, etc. [9–11], while the treatment of antibiotics in human feces and urine (black water) remains challenging [12–14]. Since most black water enters sewage treatment plants from septic tanks, the sewage treatment plant is the last barrier that could avoid spilling antibiotics into natural waters efficiently. However, conventional treatment processes such as coagulation and sedimentation remove mainly contaminants such as nitrogen, phosphorus and organic matter, but not antibiotics [15–17]. Levels of antibiotics during wastewater treatment may increase and promote antibiotic resistance among bacteria in the receiving environment [18,19]. Alternatively, membrane filtration [20], advanced oxidation [21], and adsorption [22] have been applied to remove antibiotics from wastewater. Yet some shortcomings such as membrane fouling and the production of secondary contaminants still remain [23]. These issues may be solved by the recent development of photocatalytic membranes, which are more stable, efficient and hydrophilic [24], in particular by using the TiO_2 photocatalyst [25]. Abellan et al. conducted a photocatalytic degradation of SMZ by TiO_2 and inferred the progress of the photocatalytic reaction by tracing the

* Corresponding author at: 516, Jungong Road, 200093 Shanghai, China.
E-mail address: Liuhb@usst.edu.cn (H. Liu).

concentration of various ions in water [26]. The results showed that SMZ was mineralized to CO_2, H_2O, and other harmless salt ions at the end of the photocatalytic reactions.

TiO_2 modification membranes have been recently synthesized because of their special hydrophilicity, chemical stability, non-toxicity and ability to change the physical and chemical characteristics of polymeric films. Vatanpour et al. embedded TiO_2-coated multi-walled carbon nanotubes in polyethersulfone material to form photocatalytic membranes and to improve membrane contamination by increasing the hydrophilicity of the membrane and reducing the surface roughness of the membrane [27]. Razmjou A et al. modified TiO_2 nanoparticles by silane coupling agent KH-550 and subsequently used the resulting TiO_2 particles to prepare composite membranes with PES (Polyethersulfone), indicating that the modified TiO_2 co-blended membranes improved the contamination resistance of PES effectively [28]. Wang et al. immobilized anatase phase TiO_2 photocatalyst on the membrane; the modified membrane presented good photocatalytic activity and was able to degrade, even mineralize phenol to CO_2 under the UV light irradiation [2].

To broaden the light driving range of TiO_2 and reduce the band gap energy of TiO_2 for photocatalysis under visible light, g-C_3N_4 was used to reduce the band gap energy of TiO_2 [29]. The material g-C_3N_4 is of good chemical and thermal stability, with low cost and non-toxic properties [30], which could be synthesized to enhance the removal efficiency of photocatalytic materials with more extensive application aspects. In addition, previous studies have shown that the energy level positions of g-C_3N_4 and TiO_2 match well so that TiO_2 can accept the electrons from g-C_3N_4 [31,32].

Here we synthesized and tested the membrane made by *co*-blending polyvinylidene fluoride (PVDF) and g-C_3N_4/TiO_2 for the photocatalytic removal of SMZ and TC from simulated black water. We compared the basic membrane filtration and photocatalytic performance of g-C_3N_4/TiO_2 and PVDF membranes, and investigated the influencing factors and application aspects of membrane filtration-photocatalytic systems for antibiotic removal. The anti-fouling performance and re-usability of g-C_3N_4/TiO_2 membranes were investigated by evaluating the fouling reversibility of photocatalytic membranes. Following that, it provides new implications and application methods for the removal of trace antibiotics.

2. Materials and methods

2.1. Preparation and characterization of g-C_3N_4/TiO_2 membranes

2.1.1. Preparation of g-C_3N_4/TiO_2 photocatalytic particles

Appropriate amounts of melamine and butyl titanate were weighed and prepared as the g-C_3N_4/TiO_2 precursor by the sol-gel method. The precursor was baked in a muffle furnace at 550 °C for 4 h to obtain a pale yellow lumpy solid. The resulting product was ground by a ball mill to obtain homogeneous g-C_3N_4/TiO_2 photocatalytic particles.

2.1.2. Preparation of g-C_3N_4/TiO_2 membranes

A certain amount of N-N-dimethylacetamide (DMAc) was placed in a conical flask, mixed with an appropriate amount of g-C_3N_4/TiO_2 powder, sonicated at room temperature for 30 min, and then the polyvinylpyrrolidone (PVP) and PVDF powder were dosed after uniform dispersion. The mixed samples were put into a water bath and heated until the solution was transparent, then mechanically stirred in a water bath at 65 °C for 12 h and left to stand at constant temperature for 12 h to form a cast membrane solution.

The ultrafiltration membrane was prepared by the submerged precipitation phase conversion method. The membrane casting solution was poured evenly and slowly onto a glass plate in the form of strips. The thickness of the squeegee was adjusted to 200 μm and the membrane was squeegeed at a uniform speed of 2 cm/s. After standing for 30 s at room temperature (about 25 °C), the glass plate coated with the cast membrane solution was quickly cut into room-temperature deionized water at an oblique angle, then placed flatly until the cast membrane solution changed from the liquid to the solid phase. When the solid membrane can be freed from the glass, the membrane is removed and placed in room-temperature deionized water for 24 h to ensure full solvent replacement and evaporation, then the membrane is rinsed with deionized water and stored in fresh deionized water. The surface of the membrane is rinsed with deionized water before each experiment to remove the residual cast membrane solution.

The PVDF-2 membrane (PVDF: PVP: DMAC = 20:3:77) was chosen as the basis of the photocatalytic modified membrane, after which five kinds of g-C_3N_4/TiO_2 membranes were further prepared. The specific ratios of membrane materials are shown in Table S1.

2.1.3. Characterization of g-C_3N_4/TiO_2 membranes

After freeze-drying the composite membranes, the hydrophilicity of the composite membranes was tested by the contact angle meter (Chengde Dingsheng Testing Machine Testing Equipment Co. JY-82, China). Scanning electron microscopy (SEM) (ZEISS Gemini 300, Germany) was used to study the surface morphology characteristics and pore formation of the photocatalytic membranes.

2.2. Build-up of the membrane filtration-photocatalysis system

2.2.1. Dead-end filtration

The experimental setup consisted of a MSC300 ultrafiltration cup from Shanghai Mosel, a constant pressure system including a nitrogen bottle and pressure gauge, and a magnetic stirrer. Firstly, the membrane was placed at the bottom of the cup ultra-filter, 200 mL of deionized water was added to the device, and then the filtration experiment was carried out at a constant pressure of 0.1 Mpa. Once the effluent flow rate is stable, the time taken for the same volume change is recorded. The membrane flux is then calculated according to the change of volume with time.

2.2.2. The membrane filtration-photocatalysis system

The photocatalytic filtration apparatus is shown in Fig. S1. Artificial water containing antibiotics was injected into the cup at the upper end of the membrane assembly and put in darkness for 1 h away from light. After the photocatalytic membrane reached adsorption and desorption equilibrium, a light filtration experiment was performed under 0.1 Mpa contraction pressure and 300 W xenon lamp irradiation.

The composition of the simulate mixed black water is prepared according to previous analytical studies of real mixed black water components with properties listed in Table S2 [33].The original concentrations of TC and SMZ were both 50 μg/L and the characteristics of the artificial black water containing antibiotics were listed in Table S3. All experiments were performed at room temperature (about 25 °C) with samples taken at 30-min intervals, purged with nitrogen and then re-dissolved and processed for quantification by a liquid chromatograph-mass spectrometer (LC-MS) (Text S1).

2.3. Performance of the membrane filtration-photocatalysis system

2.3.1. Membrane flux

For each filtration test, experiments were started by firstly running with deionized water for 1 h to rinse out the impurities of the membrane. After the effluent flux was stabilized, the time spent per unit volume was measured and the initial flux of the membrane, J_0, was calculated according to the following eq. (1).

$$J_0 = \frac{V}{St} \tag{1}$$

where: J_0 is the membrane flux in L/(m^2·h); V is the filtration volume in L; S is the effective filtration area in m^2, and t is the filtration time per

unit volume in h.

2.3.2. Membrane retention rate

Membrane retention performance was measured using 500 mg/L bovine serum albumin (BSA) as the retention contaminant. The filter solution was measured by a UV spectrophotometer at the absorbance of 283.4 nm, and the concentration of BSA before and after filtration was calculated from the standard curve of BSA (y = 0.0006×-0.0027), and the retention rate R was calculated by eq. (2).

$$R = \left(1 - \frac{C2}{C1}\right) \times 100 \quad (2)$$

where: R is the BSA retention rate of the filter membrane, %; C_1 is the concentration of BSA before filtration, mg/L; C_2 is the concentration of BSA after filtration, mg/L.

2.3.3. Porosity test

The ultrafiltration membrane was simply treated and its wet weight (W_W) and dry weight (W_D) were determined using an electronic balance to obtain the porosity(P_r) of the membrane according to eq. (3) [34].

$$P_r = \frac{W_W\text{-}W_D}{\rho_{H_2O} \cdot V} \times 100\% \quad (3)$$

In this equation, P_r is the porosity; W_D is the weight (g) of the ultrafiltration membrane after it has been subject to freeze-drying for 24 h; Ww is the weight of the ultrafiltration membrane after 24 h soaking in deionized water and wiped off the residual water on the surface; ρ is the density of water with the value of 1 g/cm^3, and V is the dry membrane volume (cm^3).

2.4. Effect of water quality characteristics on antibiotic removal

We set the antibiotic solution concentrations to 50 μg/L, 100 μg/L and 150 μg/L for the study of the effect of initial concentration on the antibiotic removal rate. We adjusted the antibiotic solution by 1 M NaOH and HCl to pH 1.0, 3.0, 5.0, 7.0 and 9.0 respectively to conduct the study of the effects of pH on the antibiotic removal rate, and explored the practical application of g-C_3N_4/TiO_2 membrane with investigations on black water treatments. All the above studies were carried out by a membrane filtration-photocatalysis system at a light intensity of 150 mW/cm^2, a light duration of 150 min, and a pressure of 0.1 Mpa.

2.5. Mechanism study on degradation of antibiotics

The main active species in the photocatalytic process are hydroxyl radicals (·OH), superoxide radicals (·O_2-) and photogenerated holes (h^+). We used quenching experiments to identify the main active species during the photocatalytic degradation of SMZ and TC. The addition of 0.01 mol/L ethanol and EDTA-2Na to 50 μg/L antibiotic solutions was applied to quench ·OH and h^+ respectively [35]; the introduction of nitrogen to the antibiotic solution was to reduce dissolved oxygen in the water column and inhibit ·O_2- production [36].

2.6. Contact angle measurement (sessile-drop method)

Water contact angle was measured with a Data Physics optical contact angle measuring instrument, with the droplet size controlled using a Gilmont syringe. A drop of liquid was added to the treated membrane surface, and the wettability of the liquid to the solid was reflected by measuring the angle between the two tangents of the gas-liquid interface and the solid-liquid interface on the membrane surface. The hydrophilic changes of the PVDF and the g-C_3N_4/TiO_2 membranes were thus compared. All measurements were carried out at room temperature.

3. Results and discussion

3.1. Characterization of the g-C_3N_4/TiO_2 modified membranes

The composition of the membrane affects its surface morphology and pore structure, altering its hydrophilicity. As revealed in Fig. 1, all membranes tested have a typical asymmetric structure with obvious dense layers, porous support layers and microporous structures. With the increase of PVP (Polyvinylpyrrolidone) and the addition of g-C_3N_4/TiO_2 particles, the number of membrane pores increased significantly, and the pore distribution was more uniform. Both PVDF-2 and PgT-3 membranes have a regular finger-like pore structure, but the pore channels of PgT-3 membrane are larger, which could enhance the flux of the membrane [37]. During the formation of PgT-3 membrane, hydrophilic g-C_3N_4/TiO_2 migrates to the membrane surface, forming a thinner dense layer than the PVDF-2 membrane, and the hydrophilicity of the membrane surface increases. The AFM image (Fig. S2) shows that after the addition of g-C_3N_4/TiO_2 particles, the degree of concavity of the PgT-3 film was obviously improved, and the g-C_3N_4/TiO_2 particles filled into the interstices of the polymer during film formation, which reduced the roughness of the film surface. This makes the membrane surface less prone to fouling enrichment, which helps enhance the modified membrane's resistance to contamination and makes it easier to be cleaned.

FT-IR spectra of the PVDF-2 and the PgT-3 membranes was shown in Fig.S3 to investigate the effect of adding g-C_3N4/TiO_2 photocatalytic particles on the structure of functional groups of the surface membrane. The characteristic peak near 2942.94 cm^{-1} corresponds to the characteristic vibrational peak of -OH. Due to the addition of photocatalytic particles, the -OH content increased and the peak of the Pgt-3 membrane was slightly enhanced compared to the PVDF membrane, which is one of the main reasons for the increase in membrane hydrophilicity and pure water flux. The intensity of the characteristic peaks associated with the membrane composition of the Pgt-3 membrane was slightly decreased compared with that of the PVDF membrane, indicating that the addition of g-C_3N_4/TiO_2 photocatalytic particles changed the properties of the

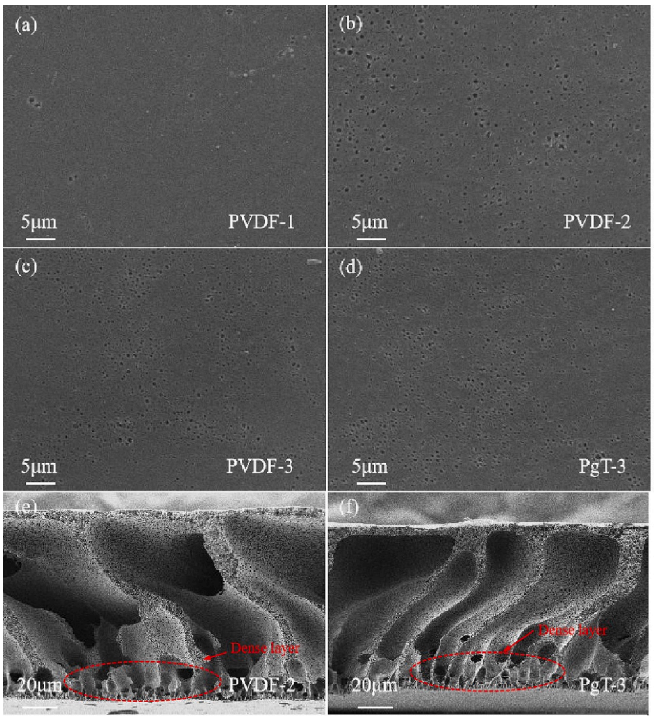

Fig. 1. SEM images of the (a) PVDF-1 membrane; (b) PVDF-2 membrane; (c) PVDF-3 membrane; (d) PgT-3 membrane and cross-section SEM images of the (e) PVDF-2 membrane and (f) PgT-3 membrane.

PVDF membrane.

The UV–Vis absorption spectra in Fig.S4 were used to confirm the optical absorption properties of the PVDF-2 and the PgT-3 membranes. The absorption wavelength of TiO_2 is around 390 nm, which corresponds to a forbidden band width of 3.22 eV, and the main absorption wavelength size of g-C_3N_4 nanoparticles is around 470 nm, which corresponds to a forbidden band width of 2.74 eV. By the tangent method, the absorption edge of g-C_3N_4/TiO_2 can be obtained to be about 590 nm, which is significantly different to the case of TiO_2. The absorption band extends from the UV region (10–400 nm) to the visible region (400–760 nm) and shows strong visible absorption due to the reduction of the band gap. The band gap of energy (Eg) size of g-C_3N_4/TiO_2 photocatalytic particles is 2.45 eV. It has been shown that when the content of polytriazine crystal layer in g-C_3N_4/TiO_2 is high, crystalline organic semiconductor layers can be bonded with Ti^{4+} and form specific semiconductor heterojunctions through Ti-N-C bonds. Semiconductor heterojunctions change the forbidden band width of the semiconductor material, transfer photoelectrons to TiO_2, and broaden the light response range, so that the visible light can excite g-C_3N_4/TiO_2 to produce electrons and degrade pollutants.

Fig. 2a shows the changes in contact angle and porosity. It can be seen that the contact angles of the modified membranes with the addition of g-C_3N_4/TiO_2 particles are all smaller than that of the base membranes, which decreases with the increase of g-C_3N_4/TiO_2 addition. The addition of g-C_3N_4/TiO_2 can significantly improve the hydrophilicity and wettability of the membrane [38]. However, when the dosing amount of g-C_3N_4/TiO_2 exceeds 0.03 wt%, the contact angle of the membrane surface increases slightly with the increase of the dosage, but it still has better hydrophilicity compared with the PVDF-2 membrane. Fig. 2a indicates that an overdose of photocatalytic particles (>3) made the presence of g-C_3N_4/TiO_2 particles in the cast membrane solution unable to disperse and form partial agglomerates, resulting in a reduction of the overall surface area compared with the dispersion of particles and a reduction of the exposed hydrophilic groups, thus increased the contact angle of the membrane surface and reduced its hydrophilicity.

The larger the porosity of membranes leads to the better the water permeability of the ultrafiltration membrane and the higher the pure water flux. The porosity of the PgT-3 membrane is 61.4 %, which presents the largest porosity among the modified membranes. It can be speculated that the addition of hydrophilic particles g-C_3N_4/TiO_2 promotes the interpenetration and exchange of water and solvent in the cast membrane solution, and the rapid phase separation facilitates the formation of finger-like macropores. The curing process of membrane formation produces a delayed phenomenon, which increases the porosity of the membrane. The increase of solute leads to the increase of viscosity of the cast membrane solution, which hinders the interpenetration of water and solvent when converting into membrane, preventing the formation of finger-like macropores and decreasing the porosity.

Fig. 2b depicts the magnitude of membrane flux and retention rate for eight study membranes. The pure water fluxes of the modified membranes were all significantly higher than that of the base membranes. The highest pure water flux was achieved with the PgT-3 membrane with 0.03 wt% g-C_3N_4/TiO_2 addition at 647.89 L/(m^2·h), which was 65.7 % higher than that of the PVDF-2 membrane without the addition of photocatalytic particles.

With the increase of photocatalytic particle addition, the change of modified membrane pure water flux showed a trend of first increasing and then decreasing, which corresponded to the results of porosity detection. When the addition amount exceeded 0.03 wt%, the pure water flux of the modified membrane showed a first decrease phase, which was presumed to be caused by the aggregation of photocatalytic particles in combination with the cross-sectional SEM image of the modified membrane. On the one hand, the aggregation of photocatalytic particles affects the structure of the g-C_3N_4/TiO_2 modified membrane, leading to a slowing down of the filtration process; on the other hand, the reduction of the specific surface area of the particles reduces the hydrophilic groups and decreases the hydrophilicity of the membrane surface. Both the PVDF-2 and the g-C_3N_4/TiO_2 modified membranes retained BSA in the range of 80–85 %, indicating that the addition of g-C_3N_4/TiO_2 had a limited effect on the retention of BSA by the modified membranes. The performance characterization of the membranes showed that the PgT-3 modified membranes exhibited good hydrophilicity, permeability, and separation properties.

The chemical composition and valence state of elements in the PgT-3 membrane were identified by the XPS survey spectra (Fig. S5). Fig. S5a presents the full survey XPS spectrum of the representative PgT-3 sample, which clearly indicates that the PgT-3 is mainly composed of C, N, Ti and O elements. Fig. S5b shows that the sample has three C1s peaks located at 284.8 eV, 286.3 eV and 288.4 eV, which attribute to sp^2 C—C, sp^3 C—N and sp^2 C═N, respectively. Fig. S5c shows three N1s peaks located at 398.5 eV, 400.0 eV and 401.0 eV, which attribute to aromatic N(C=N-C), N-$(C)_3$ and -NH_2, respectively. Fig. S5d was the high-resolution spectrum of Ti 2p of the PgT-3 sample, which can be assigned to Ti $2p_{3/2}$ and Ti $2p_{1/2}$, respectively. This result also confirms that the as-prepared sample is a composite of TiO_2 and g-C_3N_4.

3.2. *Performances of the membrane filtration-visible light photocatalytic system*

The effects of the g-C_3N_4/TiO_2 concentration for membrane

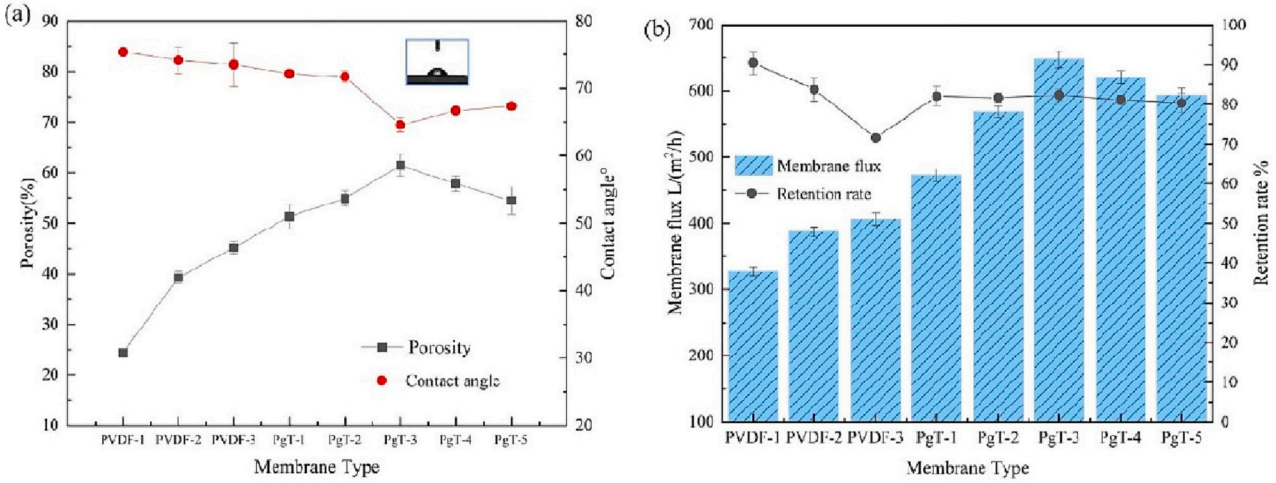

Fig. 2. Characterization of eight membranes in terms of (a) Contact angle and porosity, and (b) Membrane flux and retention rate.

modification on the removal of SMZ and TC was tested under 150 W visible light irradiation (Fig. 3). The initial concentrations of SMZ and TC were both 50 mg/L. After 150 min, the removal rate of SMZ increased from 55.3 % to 72.8 %, with g-C_3N_4/TiO_2 concentration for membrane modification increased from 0.01 % to 0.03 %. Then the SMZ removal rate decreased to 59.0 % when the g-C_3N_4/TiO_2 concentration was 0.05 %. The rising removal rate is explained by an increasing number of active sites, while the declining removal rate is likely caused by the agglomeration of photocatalytic materials, which altered its light transmission rate and contact area. We observed similar trends for TC. For example the highest removal rate also appears at 0.03 % concentration of g-C_3N_4/TiO_2 for membrane modification, though with fewer difference gaps.

The removal of SMZ and TC with an initial concentration of 50 μg/L was conducted by the PVDF membrane, the g-C_3N_4/TiO_2 modified membrane without light and the g-C_3N_4/TiO_2 membrane with light (Fig. 4). Results show that the highest removal rates of 70.8 % for SMZ and 62.1 % for TC are achieved for the g-C_3N_4/TiO_2 membrane after exposure to light for 150 min. Without light exposure, the removal rate is lower, with 40.7 % for SMZ and 44.2 % for TC respectively. By contrast, the removal rate is much lower for the PVDF membrane without g-C_3N_4/TiO_2 modification and light exposure, with 13.3 % for SMZ and 11.9 % for TC respectively. These findings imply that the addition of g-C_3N_4/TiO_2 to the membrane highly improves its removal capacity on antibiotics. This is explained by the higher porosity and hydrophilicity of the g-C_3N_4/TiO_2 membrane, which favors its contact with water-soluble antibiotics. The further removal rate on antibiotics increases with light is probably due to photocatalytic transformation of antibiotics into more polar compounds that are better adsorbed to the modified membrane. This hypothesis is supported by literature reporting that singlet molecular oxygen $^1O_2$ is generated in TC solutions under simulated sunlight, and the reactive oxygen species further promotes the degradation of antibiotics [39]. Overall, the addition of g-C_3N_4/TiO_2 highly increased the removal of antibiotics, and the application of light further increased its removal rate.

3.3. Role of major water indicators affecting removal of antibiotics by the PgT-3 modified membrane

Fig. 5a, b presents the removal rates of SMZ and TC under different initial concentrations with the PgT-3 membrane. The removal rate of antibiotics decreased gradually with the increase of initial concentrations. The removal rates of both SMZ and TC were relatively stable at an initial concentration of 50 μg/L. At an initial concentration of 150 μg/L, the removal rates of antibiotics presented significant fluctuations and instability after 60 min of reaction. The best removal rate was achieved at an initial concentration of 50 μg/L, with the removal rate of 72.8 % for SMZ and 66.1 % for TC, respectively, which were about 10 % higher than that at the initial concentration of 150 μg/L. On the one hand, the increase of solute leads to the adsorption and retaining of more substances. Since adsorption sites are limited in membrane pores and on the membrane surface, the removal rate is relatively low. On the other hand, the adsorption of antibiotics by the pore structure of the membrane gradually increases, and the enrichment of antibiotics hinders the absorption of visible light by the g-C_3N_4/TiO_2 catalyst, thus reducing the utilization of light.

As shown in Fig. 5c, the highest removal rate of SMZ was achieved by the PgT-3 membrane at pH 5.0 (69.3 %). The removal rate increases gradually as the pH rises, and the increasing trend is declining when the solution reaches neutrality. The kpa1 of SMZ is 1.9 ± 0.3 and kpa2 is 5.7 ± 0.2. When the pH is <1.9, the main form of SMZ is existed as positive ions; when the pH rises from 1.9 to 5.7, the main existence form is in a molecular state, and when the pH exceeds 5.7, the main existence form is in negative ions. SMZ obtains stronger light absorption and higher photochemical reactivity in the molecular state, presenting easier adsorption by the g-C_3N_4/TiO_2 membrane, arousing easy electrophilic attack of strong oxidizing active species, and achieving higher decomposition efficiency. The isoelectric point of g-C_3N_4/TiO_2 is about 3.0, and the catalyst surface is negatively charged at pH 4.0–10.0. Under neutral or alkaline conditions, the adsorption capacity decreased due to electrostatic repulsion, which inhibited the subsequent photocatalytic degradation. The low removal efficiency at pH 1.0 may be due to the strong acidity of the solution, resulting in a low concentration of superoxide radicals, which is not conducive to the degradation of SMZ.

The highest degradation rate of TC reached 61.2 % when the pH was 7.0. It can be seen that with the increase in pH, the degradation rate of TC showed a trend of first increasing and then decreasing. After the g-C_3N_4/TiO_2 membrane is exposed to light, the photocatalyst inside the membrane undergoes a photoelectron leap and generates photogenerated holes, which oxidizes the OH- enriched on the catalyst surface to Hydroxyl radicals (·OH), thus initiating the photocatalytic oxidation reaction. As the pH increases, the content of ·OH increases, contributing to a faster reaction rate [34]. At the same time, the morphology of TC under different pH values is different, with positive charge on the TC surface under pH values below 3.3, negligible electrostatic effect under pH values between 3.3 and 7.7, and negative charge on the TC surface at

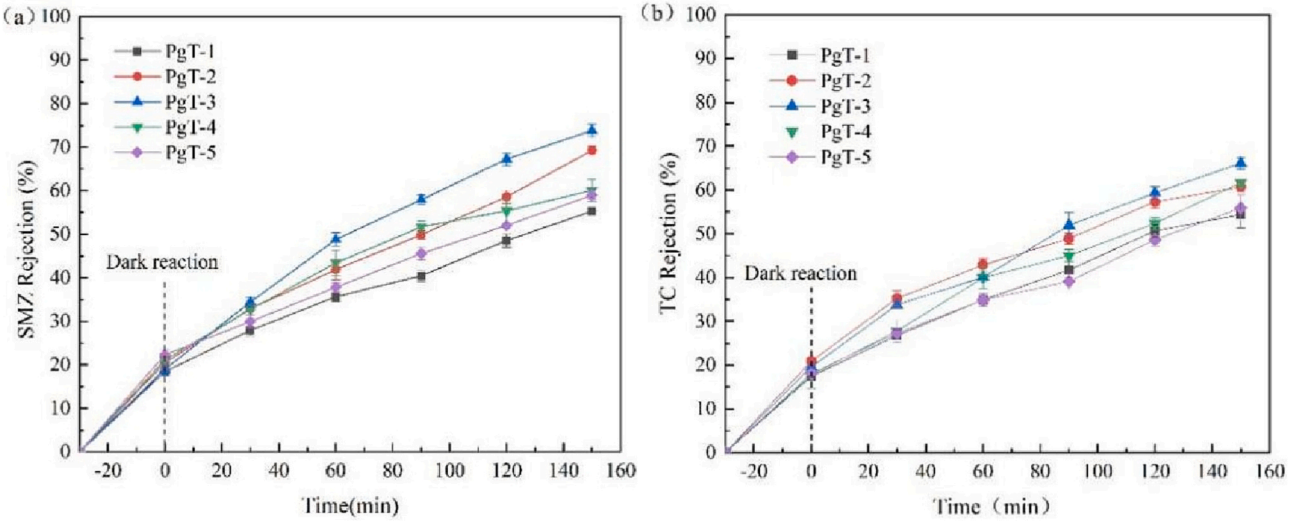

Fig. 3. Removal of antibiotics by the g-C_3N_4/TiO_2 membranes under visible light irradiation using (a) SMZ (Initial concentration = 50 μg/L) and (b) TC (Initial concentration = 50 μg/L) as model antibiotics.

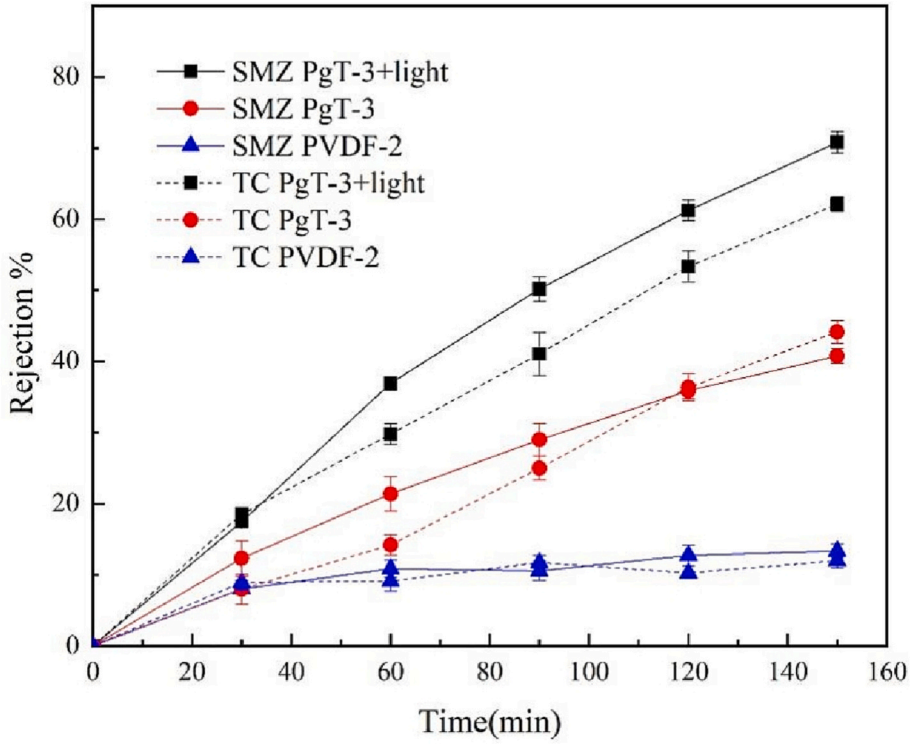

Fig. 4. Removal of SMZ (Initial concentration = 50 μg/L) and TC (Initial concentration = 50 μg/L) with the PVDF membrane, and the g-C_3N_4/TiO_2 membrane with/without light exposure.

pH values above 7.7. Some studies also showed that when the solution pH was 7.0–9.0, TC was in the anionic state and had electrostatic repulsion with g-C_3N_4/TiO_2, which inhibited the photodegradation reaction [39].

To be more representative of the real situation, we also tested the removal rate of antibiotics in simulated black water, and examined the effects of TN, TP, ammonia nitrogen, and COD in black water on performances of the photocatalytic process. According to Fig. 5d we can see that the degradation rates of SMZ and TC are significantly lower than those in Fig. 3. Specifically, after 150 min of reaction, the removal rates of SMZ and TC in the simulated black water were 46.1 % and 54.1 %, respectively, compared to 70.8 % and 62.1 % for the pure water. TN, TP, ammonia nitrogen and COD in black water were degraded by 38.6 %, 33.9 %, 36.5 % and 40.5 %, respectively. After the reaction time reached 90 min, the degradation rate of each pollutant slowed down significantly, especially for TN, TP, ammonia nitrogen and COD. The pollutant composition of black water is complex, which brings about membrane pollution and flux decline. The continuous high pressure of the system will increase the pressure difference across the membrane in case of membrane clogging, which will cause damage to the membrane structure and lead to the loss of certain g-C_3N_4/TiO_2 photocatalyst. The enrichment of pollutants in the membrane pores also greatly affects the absorption of visible light by the photocatalyst, which hinders the photocatalytic oxidation process and slows down the removal of pollutants. Meanwhile, the pH of the simulated blackwater is around 7.0–8.0, which is not favorable for the removal of SMZ and TC. The complex composition of the black water can change the charge distribution on the surface of g-C_3N_4/TiO_2 and affect the interaction between the photocatalyst and the contaminants. The decomposition and interactions of some organic substances and inorganic substances such as bicarbonate in water may trap strong oxidizing species, thus reducing the strong oxidizing groups available for photocatalytic processes and inhibiting the photocatalytic activity to hinder the reaction process of photocatalytic oxidation.

Over nine successive cycles, the removal of SMZ and TC by the PgT-3 membrane showed a steady state (Fig. 5e,f), which is similar to the findings of other researchers [40,41]. This may be due to the removal of residual organic components in the membrane pores and other contaminants attached to the membrane pore structure after prolonged light exposure and multiple hydraulic flushes. As shown in Fig. S6, the alkaline detergent configured with sodium hydroxide was more effective than the acid detergent configured with hydrochloric acid, and the higher the alkalinity, the better the cleaning effect on the membrane. When the pH value was 10.0, the cleaning effect was the best and the recovery of membrane pure water flux was 85.3 %. After cycling, it can be determined that both the PVDF and the g-C_3N_4/TiO_2 modified membranes have good reusability and stable membrane filtration capacity.

3.4. *Mechanism of SMZ and TC removal in the system*

To investigate the mechanism of antibiotic removal by the membrane filtration-photocatalytic system, we used separate masking of free radicals to identify the photocatalytically active species that play a major role in the reaction process.

As can be seen in Fig. 6a, there was a different degree of decrease in antibiotic removal for the remaining three groups compared to the control group. When EDTA-2Na and nitrogen gas were applied to the membrane filtration-photocatalytic system, the removal rates of SMZ and TC decreased to 20.9 % and 35.7 %, respectively, which was greater compared with the addition of ethanol to the system, indicating that the main active species for the degradation of SMZ was $\cdot O_2^-$ and h^+, and h^+ was the greater contributor. In Fig. 6b, the degradation effect of TC was basically the same as that of SMZ, and again the effect of h^+ on the photocatalytic degradation process was greater. At the same time, it can be seen that the removal rate of both antibiotics by the system with the addition of ethanol decreased by <10 %, indicating that the contribution of ·OH generated by the modified membrane during the photocatalytic process was limited. The forbidden band widths of g-C_3N_4 and TiO_2 are about 2.73 eV and 3.18 eV, respectively [42]. When the photocatalyst g-

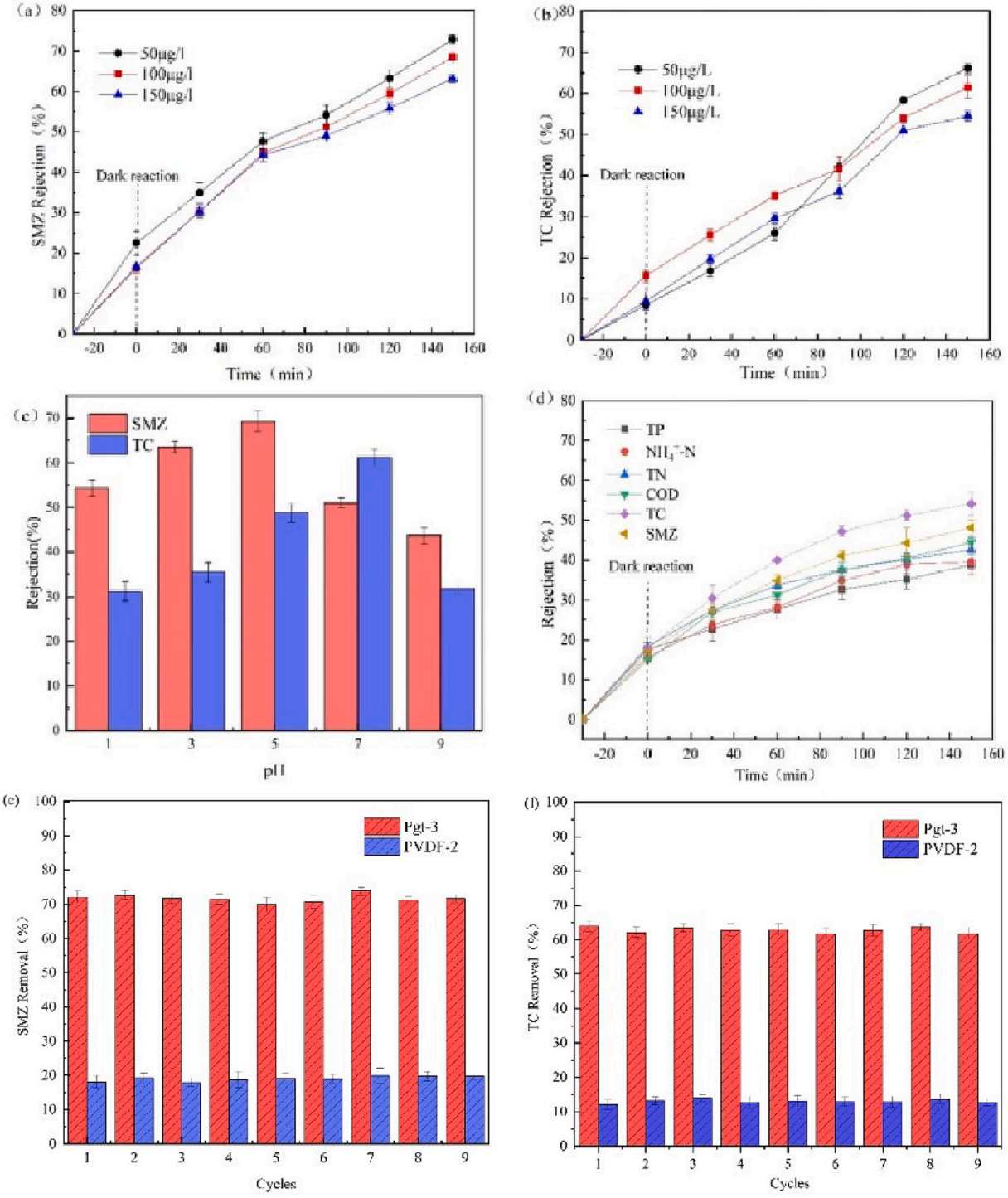

Fig. 5. (a) Effect of initial concentrations on the degradation of SMZ; (b) Effect of initial concentrations on the degradation of TC; (c) Effect of pH on antibiotic removal by modified membranes; (d) Performance of photocatalytic filtration treating black water; (e) The durability of PgT-3 for SMZ removal after several cycles and (f) The durability of PgT-3 for TC removal after several cycles.

C_3N_4/TiO_2 is irradiated by visible light, g-C_3N_4 could readily absorb visible light due to its narrow-forbidden band width. Through the tight contact interface, electrons are rapidly transferred from the conduction band (CB) of g-C_3N_4 to the CB of TiO_2, resulting in the excitation of photogenerated electron-hole pairs and the generation of photo-generated electrons. Although both g-C_3N_4 and TiO_2 have the ability to produce $\cdot O_2^-$ radical for $O_2/\cdot O_2^-$ (−0.046 eV vs NHE). The lower CB makes O_2 tend to react with the electrons from g-C_3N_4 to form $\cdot O_2^-$. The photogenerated electrons migrated from the conduction band of g-C_3N_4 to the conduction band of TiO_2, and generated $\cdot O_2^-$ by reacting with dissolved oxygen on the surface of TiO_2; while $\cdot O_2^-$ can generate ·OH directly or indirectly [43]. The electron leap is accompanied by the generation of corresponding photogenerated holes in the valence band, which can directly oxidize the antibiotics adsorbed on the surface of the photocatalyst. However, due to the low value of the valence band of g-C_3N_4, the holes remaining in the valence band can hardly be oxidized to produce the ·OH radical. Therefore, the contribution of ·OH to the removal of antibiotics from the system is small.

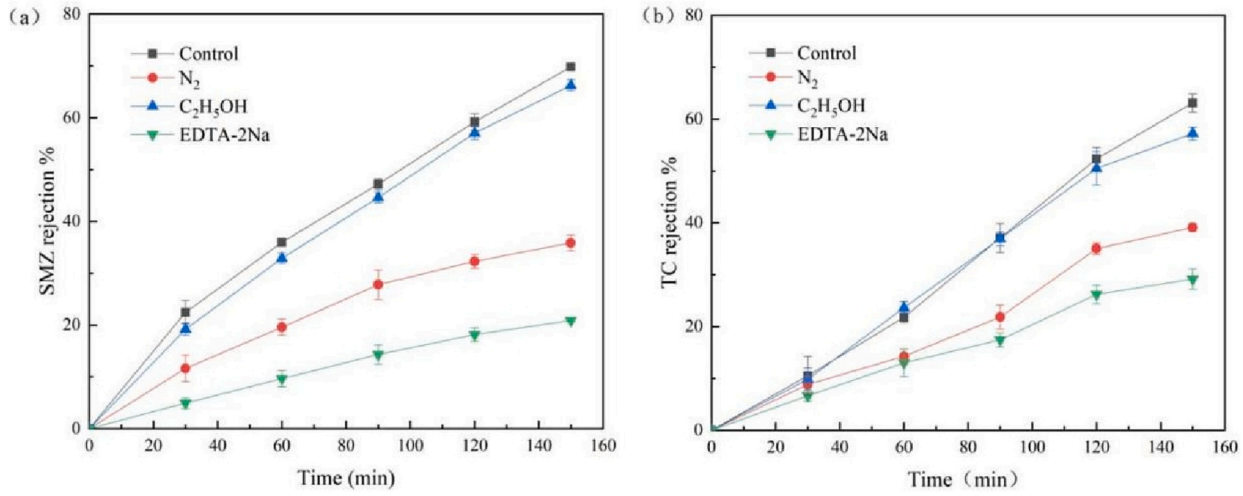

Fig. 6. Antibiotic removal rates by the PgT-3 membrane under different quenching agent conditions (a) SMZ and (b) TC.

It can be inferred that the photodegradation of the study may be processed as the following formulas [44,45]:

$$g - C_3N_4/TiO_2 + h\nu \rightarrow (g - C_3N_4/TiO_2) + h^+ + e^- \quad (1)$$

$$e^- + O_2 \rightarrow \bullet O_2^- \quad (2)$$

$$\bullet O_2^- + H_2O \rightarrow \bullet OOH + OH^- \quad (3)$$

$$2 \cdot OOH \rightarrow O_2 + H_2O_2 \quad (4)$$

$$H_2O_2 + Vis \rightarrow 2 \cdot OH \quad (5)$$

$$h^+, \bullet O_2^-, \cdot OH + SMZ + TC \rightarrow CO_2 + H_2O + Organic/inorganic\ small\ molecule \quad (6)$$

where h^+ played an important role in removing antibiotics with the PgT-3 membrane filtration-photocatalysis process. The introduction of g-C_3N_4/TiO_2 to the system poses an obvious response to visible light, which promotes the separation of electrons and holes and generates more h^+ so that the catalytic activity is improved.

4. Conclusion

The Pgt-3 membrane with 0.03 wt% of g-C_3N_4/TiO_2 performs best removing antibiotics from black water. Both the initial concentration of antibiotics and the pH of feed water influenced the removal efficiency of the photocatalytic membrane system. The best removal effect was obtained when the initial concentration of antibiotics was low and the pH of feed water was weakly acidic. The complex pollutants in the black water aggravated the adsorption load of the membrane, hindered the light absorption of the photocatalyst in the membrane and inhibited the photocatalytic process. Therefore, the black water needs to be pretreated first to reduce the adverse effects of TN, TP and COD on the g-C_3N_4/TiO_2 membrane before using the photocatalytic membrane for polishing. The photocatalytic membrane produced a large amount of $\cdot O_2^-$, h^+ and a small amount of ·OH in the photocatalytic process, among which $\cdot O_2^-$ and h^+ played the main roles in the degradation of SMZ and TC, with more contribution of h + to the degradation process. This study provides new insights into the treatment of antibiotics in black water and also provides support and reference to the treatment of black water using the membrane filtration-photocatalytic system.

Declaration of competing interest

The authors declare that they have no known competing financial interests or personal relationships that could have appeared to influence the work reported in this paper.

Data availability

Data will be made available on request.

Acknowledgments

The authors would like to acknowledge the co-funding of this work by the Natural Science Foundation of Shanghai (No. 22ZR1443200) and the National Natural Science Foundation of China (No. 52070130).

Appendix A. Supplementary data

Supplementary data to this article can be found online at https://doi.org/10.1016/j.jwpe.2023.103605.

References

[1] C. Ma, Y. Guo, D. Zhang, Y. Wang, N. Li, D. Ma, Q. Ji, Z. Xu, Metal-nitrogen-carbon catalysts for peroxymonosulfate activation to degrade aquatic organic contaminants: rational design, size-effect description, applications and mechanisms, Chem. Eng. J. 454 (2023), 140216.
[2] S. Yang, J.S. Gu, H.Y. Yu, J. Zhou, S.F. Li, X.M. Wu, L. Wang, Polypropylene membrane surface modification by RAFT grafting polymerization and TiO2 photocatalysts immobilization for phenol decomposition in a photocatalytic membrane reactor, Sep. Purif. Technol. 83 (2011) 157–165.
[3] X.Y. Qu, C. Yin, X.H. Sun, S.S. Huang, C.F. Li, P.P. Dong, X.F. Lu, Z. Zhang, A. T. Yin, Consumption of antibiotics in Chinese public general tertiary hospitals (2011–2014): trends, pattern changes and regional differences, Plos One 13 (2018).
[4] Q.Q. Zhang, G.G. Ying, C.G. Pan, Y.S. Liu, J.L. Zhao, Comprehensive evaluation of antibiotics emission and fate in the river basins of China: source analysis, multimedia modeling, and linkage to bacterial resistance, Environ. Sci. Technol. 49 (2015) 6772–6782.
[5] M. Zhang, Y.S. Liu, J.L. Zhao, W.R. Liu, L.Y. He, J.N. Zhang, J. Chen, L.K. He, Q. Q. Zhang, G.G. Ying, Occurrence, fate and mass loadings of antibiotics in two swine wastewater treatment systems, Sci. Total Environ. 639 (2018) 1421–1431.
[6] P. John, K. Johari, N. Gnanasundaram, A. Appusamy, M. Thanabalan, Enhanced Photocatalytic Performance of Visible Light Driven TiO2/gC [Formula Omitted] N4 for Degradation of Diclofenac in Aqueous, Solution 22 (2021) 101412.
[7] C. Lee, S. Jeong, M. Ju, J.Y. Kim, Fate of chlortetracycline antibiotics during anaerobic degradation of cattle manure, J. Hazard. Mater. 386 (2020), 121894.
[8] M. Hvistendahl, PUBLIC HEALTH China takes aim at rampant antibiotic resistance, Science 336 (2012), 795-795.
[9] Y.R. Hu, L. Jiang, X.Y. Sun, J.Q. Wu, L. Ma, Y.B. Zhou, K.F. Lin, Y. Luo, C.Z. Cui, Risk assessment of antibiotic resistance genes in the drinking water system, Sci. Total Environ. 800 (2021), 149650.
[10] Y.R. Hu, L. Jiang, T.Y. Zhang, L. Jin, Q. Han, D. Zhang, K.F. Lin, C.Z. Cui, Occurrence and removal of sulfonamide antibiotics and antibiotic resistance genes in conventional and advanced drinking water treatment processes, J. Hazard. Mater. 360 (2018) 364–372.

[11] T.Q. Zhang, K.Y. Lv, Q.X. Lu, L.L. Wang, X.W. Liu, Removal of antibiotic-resistant genes during drinking water treatment: a review, J. Environ. Sci. 104 (2021) 415–429.
[12] E. Noman, A. Al-Gheethi, R. Mohamed, B. Talip, M. Al-Sahari, M. Al-Shaibani, Quantitative microbiological risk assessment of complex microbial community in prawn farm wastewater and applicability of nanoparticles and probiotics for eliminating of antibiotic-resistant bacteria, J. Hazard. Mater. 419 (2021), 126418.
[13] X. Liu, H. Wang, H.M. Zhao, Prevalence of antibiotic resistance genes in wastewater collected from ornamental fish market in northern China, Environ. Pollut. 271 (2021) 116316.
[14] C.Y. Liang, D. Wei, S.Y. Zhang, Q.H. Ren, J.P. Shi, L. Liu, Removal of antibiotic resistance genes from swine wastewater by membrane filtration treatment, Ecotoxicol. Environ. Saf. 210 (2021) 111885.
[15] L. Zhu, H. Tao, X. Dai, B. Dong, W. Zhang, Impact of hydrophilic functional groups of macromolecular organic fractions on food waste digestate dewaterability, J. Environ. Manag. 326 (2023), 116722.
[16] C.C. Ryan, D.T. Tan, W.A. Arnold, Direct and indirect photolysis of sulfamethoxazole and trimethoprim in wastewater treatment plant effluent, Water Res. 45 (2011) 1280–1286.
[17] A. Gulkowska, H.W. Leung, M.K. So, S. Taniyasu, N. Yamashita, L.W.Y. Yeunq, B. J. Richardson, A.P. Lei, J.P. Giesy, P.K.S. Lam, Removal of antibiotics from wastewater by sewage treatment facilities in Hong Kong and Shenzhen, China, Water Res. 42 (2008) 395–403.
[18] C.X. Chen, A. Aris, E.L. Yong, Z.Z. Noor, A review of antibiotic removal from domestic wastewater using the activated sludge process: removal routes, kinetics and operational parameters, Environ. Sci. Pollut. Res. 29 (2022) 4787–4802.
[19] A. Naquin, A. Shrestha, M. Sherpa, R. Nathaniel, R. Boopathy, Presence of antibiotic resistance genes in a sewage treatment plant in Thibodaux, Louisiana, USA, Bioresour. Technol. 188 (2015) 79–83.
[20] R. Janssens, M.K. Mandal, K.K. Dubey, P. Luis, Slurry photocatalytic membrane reactor technology for removal of pharmaceutical compounds from wastewater: towards cytostatic drug elimination, Sci. Total Environ. 599 (2017) 612–626.
[21] P. Karaolia, I. Michael-Kordatou, E. Hapeshi, J. Alexander, T. Schwartz, D. Fatta-Kassinos, Investigation of the potential of a membrane BioReactor followed by solar Fenton oxidation to remove antibiotic-related microcontaminants, Chem. Eng. J. 310 (2017) 491–502.
[22] J. Zhao, G.W. Liang, X.L. Zhang, X.W. Cai, R.N. Li, X.Y. Xie, Z.W. Wang, Coating magnetic biochar with humic acid for high efficient removal of fluoroquinolone antibiotics in water, Sci. Total Environ. 688 (2019) 1205–1215.
[23] S.O. Ganiyu, E.D. van Hullebusch, M. Cretin, G. Esposito, M.A. Oturan, Coupling of membrane filtration and advanced oxidation processes for removal of pharmaceutical residues: a critical review, Sep. Purif. Technol. 156 (2015) 891–914.
[24] H.B. Yu, J.H. Huang, L.B. Jiang, X.Z. Yuan, K.X. Yi, W. Zhang, J. Zhang, H.Y. Chen, Steering photo-excitons towards active sites: intensified substrates affinity and spatial charge separation for photocatalytic molecular oxygen activation and pollutant removal, Chem. Eng. J. 408 (2021) 127334.
[25] B. Gao, M. Sun, W. Ding, Z. Ding, W. Liu, Decoration of γ-graphyne on TiO2 nanotube arrays: improved photoelectrochemical and photoelectrocatalytic properties, Appl. Catal. B Environ. 281 (2021), 119492.
[26] M.N. Abellán, B. Bayarri, J. Giménez, J. Costa, Photocatalytic degradation of sulfamethoxazole in aqueous suspension of TiO2, Appl. Catal. B Environ. 74 (2007) 233–241.
[27] N. Nasrollahi, L. Ghalamchi, V. Vatanpour, A. Khataee, Photocatalytic-membrane technology: a critical review for membrane fouling mitigation, J. Ind. Eng. Chem. 93 (2021) 101–116.
[28] A. Razmjou, J. Mansouri, V. Chen, The effects of mechanical and chemical modification of TiO2 nanoparticles on the surface chemistry, structure and fouling performance of PES ultrafiltration membranes, J. Membr. Sci. 378 (2011) 73–84.
[29] P. John, K. Johari, N. Gnanasundaram, A. Appusamy, M. Thanabalan, Enhanced Photocatalytic Performance of Visible Light Driven TiO2/gC [Formula Omitted] N4 for Degradation of Diclofenac in Aqueous, Solution 22 (2021) 101412.
[30] G.P. Dong, Y.H. Zhang, Q.W. Pan, J.R. Qiu, A fantastic graphitic carbon nitride (g-C3N4) material: electronic structure, photocatalytic and photoelectronic properties, J Photochem Photobiol C: Photochem Rev 20 (2014) 33–50.
[31] X.Y. Du, X. Bai, L. Xu, L. Yang, P.K. Jin, Visible-light activation of persulfate by TiO2/g-C3N4 photocatalyst toward efficient degradation of micropollutants, Chem. Eng. J. 384 (2020) 123245.
[32] C. Zhang, H. Wang, H. Yu, K. Yi, W. Zhang, X. Yuan, J. Huang, Y. Deng, G. Zeng, Single-atom catalysts for hydrogen generation: rational design, recent advances, and perspectives, Adv. Energy Mater. 12 (2022) 2200875.
[33] S. Qin, H.B. Liu, Q.C. Meng, Y.H. Zhou, S.Y. Xu, E. Lichtfouse, Z.B. Chen, Enhanced nutrient removal from mixed black water by a microbial ultra-low weak electrical stimulated anaerobic-two stage anoxic/aerobic process, Chem. Eng. J. 434 (2022) 134615.
[34] W.U. Arifeen, M. Kim, J. Choi, K. Yoo, R. Kurniawan, T.J. Ko, Optimization of porosity and tensile strength of electrospun polyacrylonitrile nanofibrous membranes, Mater. Chem. Phys. 229 (2019) 310–318.
[35] A. Mattsson, L. Osterlund, Adsorption and photoinduced decomposition of acetone and acetic acid on anatase, brookite, and rutile TiO2 nanoparticles, J. Phys. Chem. C 114 (2010) 14121–14132.
[36] Z.J. Luo, L.L. Qu, J.Z. Jia, J. Wang, S.Y. Jiang, Z.R. Wu, X.Y. Wu, TiO2/EDTA-rich carbon composites: synthesis, characterization and visible-light-driven photocatalytic reduction of Cr(VI), Chin. Chem. Lett. 29 (2018) 547–550.
[37] E. Celik, H. Park, H. Choi, H. Choi, Carbon nanotube blended polyethersulfone membranes for fouling control in water treatment, Water Res. 45 (2011) 274–282.
[38] X.T. Zhao, N. Jia, L.J. Cheng, L.F. Liu, C.J. Gao, Dopamine-induced biomimetic mineralization for in situ developing antifouling hybrid membrane, J. Membr. Sci. 560 (2018) 47–57.
[39] S.J. Jiao, S.R. Zheng, D.Q. Yin, L.H. Wang, L.Y. Chen, Aqueous photolysis of tetracycline and toxicity of photolytic products to luminescent bacteria, Chemosphere 73 (2008) 377–382.
[40] T. Giannakopoulou, I. Papailias, N. Todorova, N. Boukos, Y. Liu, J. Yu, C. Trapalis, Tailoring the energy band gap and edges' potentials of g-C3N4/TiO2 composite photocatalysts for NOx removal, Chem. Eng. J. 310 (2017) 571–580.
[41] T.-T. Zhou, F.-H. Zhao, Y.-Q. Cui, L.-X. Chen, J.-S. Yan, X.-X. Wang, Y.-Z. Long, Flexible TiO2/PVDF/g-C3N4 nanocomposite with excellent light photocatalytic performance, Polymers 12 (2019) 55.
[42] S.P. Adhikari, G.P. Awasthi, H.J. Kim, C.H. Park, C.S. Kim, Electrospinning directly synthesized porous TiO2 nanofibers modified by graphitic carbon nitride sheets for enhanced photocatalytic degradation activity under solar light irradiation, Langmuir 32 (2016) 6163–6175.
[43] R.R. Hao, G.H. Wang, H. Tang, L.L. Sun, C. Xu, D.Y. Han, Template-free preparation of macro/mesoporous g-C3N4/TiO2 heterojunction photocatalysts with enhanced visible light photocatalytic activity, Appl. Catal. B Environ. 187 (2016) 47–58.
[44] S. Babić, A.J. Horvat, D.M. Pavlović, M. Kaštelan-Macan, Determination of pKa values of active pharmaceutical ingredients, TrAC Trends Anal. Chem. 26 (2007) 1043–1061.
[45] H.Q. Sun, S.B. Wang, H.M. Ang, M.O. Tade, Q. Li, Halogen element modified titanium dioxide for visible light photocatalysis, Chem. Eng. J. 162 (2010) 437–447.

Supplementary Material

Removal of antibiotics from black water by a membrane filtration-visible light photocatalytic system

Hongbo Liu[1*a], Haodong Zhang[a], Xinyi Dong[a], Guixia Ji[a], Chengyang Wu[a], Eric Lichtfouse[b]

a School of Environment and Architecture, University of Shanghai for Science and Technology, 516 Jungong Road, 200093, Shanghai, China. b Aix-Marseille Univ, CNRS, IRD, INRA, Coll France, CEREGE, 13100 Aix en Provence, France

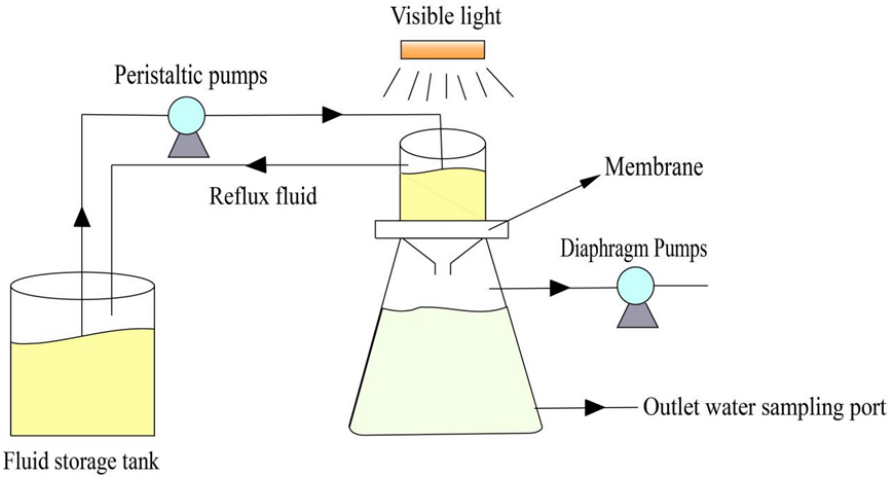

Figure S1 The membrane filtration-photocatalysis system

1* Corresponding author ADD: 516, Jungong Road, 200093, Shanghai, China;
Email: Liuhb@usst.edu.cn (H., Liu); Tel: +86(21)55275979; Fax: +86(21)55275979

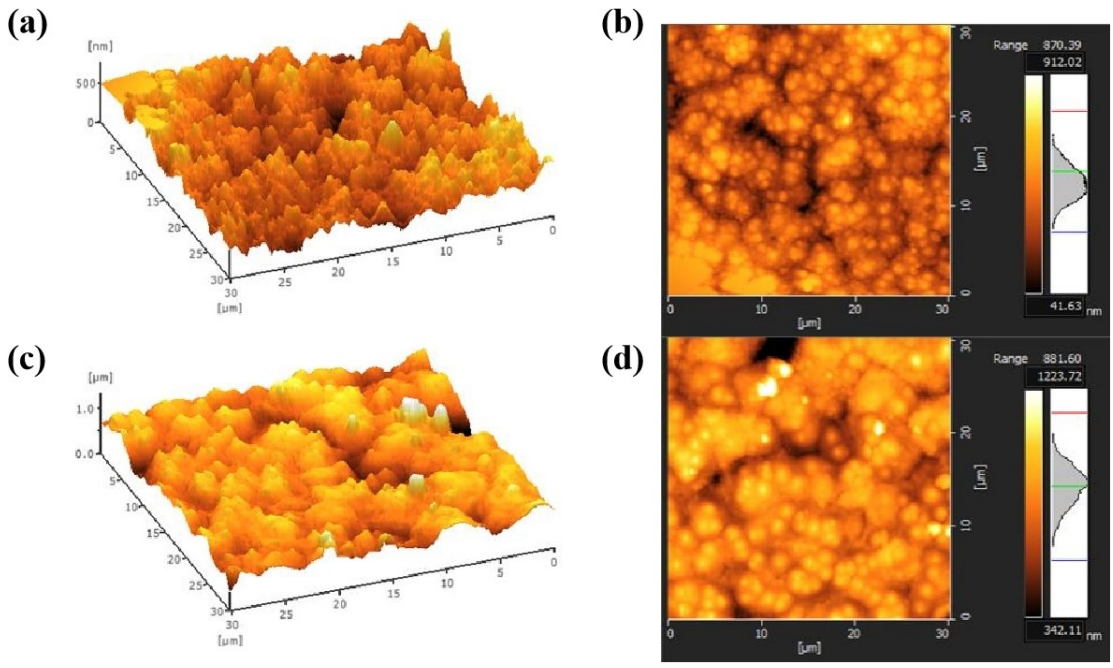

Figure S2 AFM images of PVDF-2 and PgT-3 membranes (a) 3D image of PVDF-2 membrane (b) 2D image of PVDF-2 membrane (c) 3D image of PgT-3 membrane (d) 2D image of PgT-3 membrane. During membrane application, contaminants tend to accumulate in the low valley, and the unevenness of the membrane surface will aggravate the membrane contamination. After the addition of g-C_3N_4/TiO_2 particles, the convexity of PgT-3 membrane is obviously improved. g-C_3N_4/TiO_2 particles fill the interstices of the polymer during membrane formation, which reduces the roughness of the membrane surface and makes the membrane surface flatter and smoother. Therefore, contaminants are not easily enriched on the membrane surface to form fouling, which helps to enhance the anti-pollution ability of the modified membrane and makes it easier to clean.

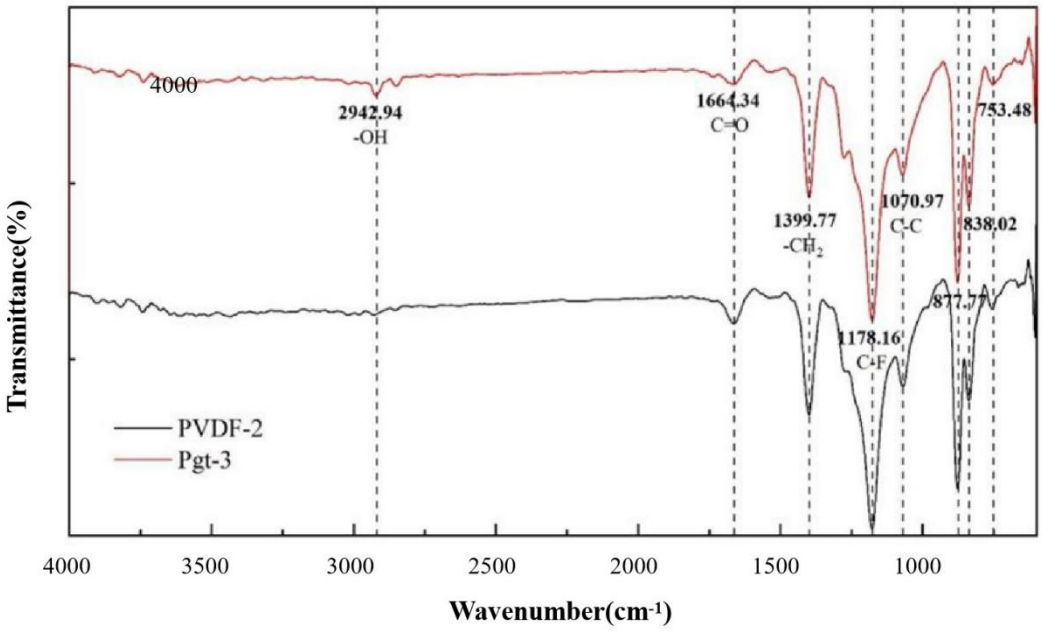

Figure S3 FTIR spectra of PVDF-2, and Pgt-3 membranes

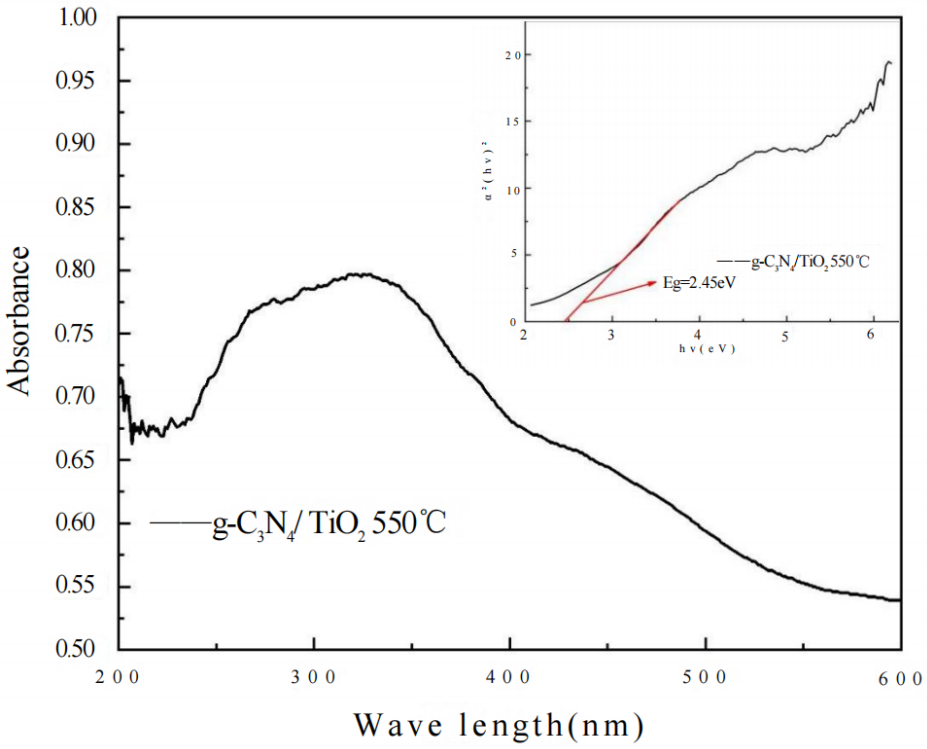

Figure S4 UV-vis plots and $\alpha^2(hv)^2$ vs. photon energy (hv) plots of g-C_3N_4/TiO_2 photocatalytic particles

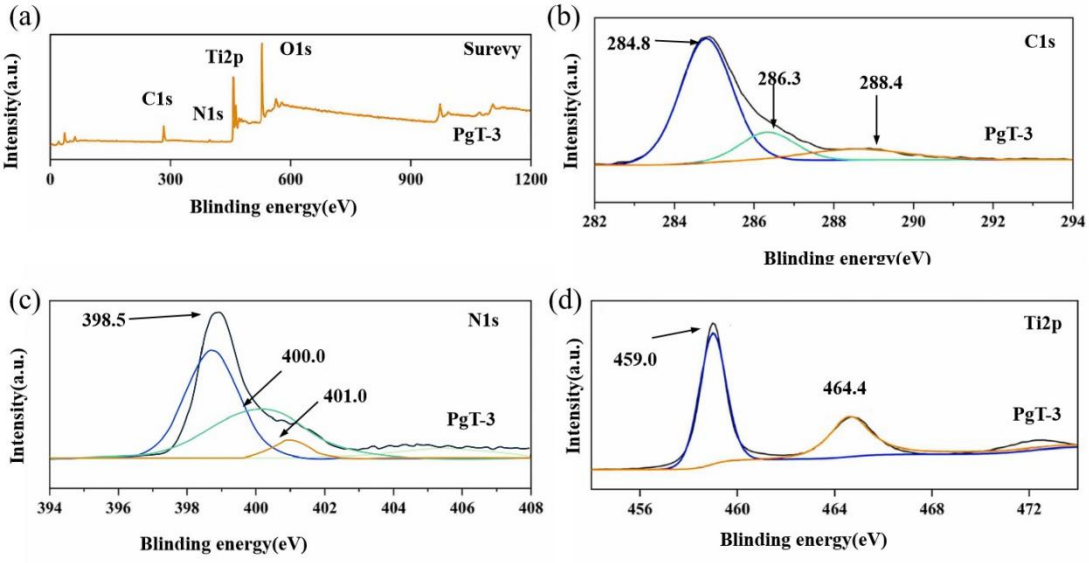

Figure S5 XPS spectrum of the representative PgT-3 sample

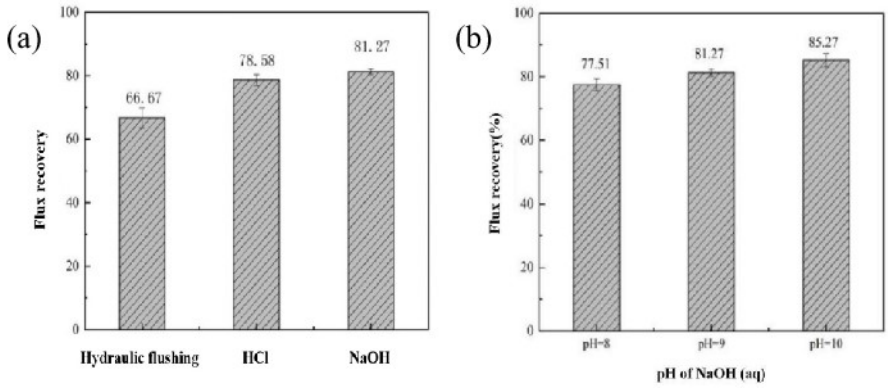

Figure S6 (a) Recovery of membrane flux under different cleaning methods; (b) Recovery of membrane flux under different H alkaline solution cleaning

Table S1 Composition of 8 types of membrane materials studied

Membrane types		Mass percentage（%）			
		PVDF	PVP	DMAc	g-C_3N_4/TiO_2
PVDF membrane	PVDF-1	20	1	79	0
	PVDF-2	20	3	77	0
	PVDF-3	20	5	75	0
The g-C_3N_4/TiO_2 membrane	PgT-1	19.99	3	79	0.01
	PgT-2	19.99	2.99	79	0.02
	PgT-3	19.99	2.99	78.99	0.03
	PgT-4	19.98	2.99	78.99	0.04
	PgT-5	19.98	2.98	78.99	0.05

Table S2 Composition of real mixed black water

Water quality index	Concentration
COD	1100±50
NH_4^+-N	55.00± 5.00
TN	55.00± 5.00
TP	10.00 – 12.00
PO_4^{3-}-P	10.00 – 12.00
pH	6.7 – 8.8

Real mixed black water samples were taken from the septic tank of a teaching building in University of Shanghai for Science and Technology (old campus at East Guoshun Road). Quality of the actual mixed black water is determined each week since year 2015.The approximate composition of artificial wastewater is in mg/L: COD 1050 – 1150, ammonia nitrogen (NH_4^+-N) 50 – 60, total nitrogen (TN) 50 – 60, and phosphate (PO_4^3-P) 10 – 12.

Table S3 Composition of artificial simulated wastewater

Ingredient	Concentration
$C_6H_{12}O_6$	0.462g/L
$C_2H_3NaO_2 \cdot 3H_2O$	1.068g/L
NH_4Cl	0.192g/L
KH_2PO_4	0.044 g/L
$NaHCO_3$	0.05g/L
$CaCl_2$	0.005g/L
$MgSO_4 \cdot 7H_2O$	0.005g/L
Trace elements	1 mL/L
Sulfamethoxazole	50 μ g/L
Tetracycline	50 μ g/L

The components of the concentrated solution of trace elements are 0.90mg/L $FeCl_3$,0.12mg/L$ZnSO_4 \cdot 3H_2O$,0.06mg/L$NaMoSO_4 \cdot 2H_2O$,0.06mg/L$MnCl_2 \cdot 4H_2O$,0.18mg/L KI ,0.03mg/L $CuSO_4 \cdot 5H_2O$,0.15mg/L $CaCl_2 \cdot 6H_2O$ and 0.15mg/L H_3BO_3.

Table S4 Evaluation parameters of the two target antibiotic detection methods

Antibiotics	Standard Curve	R^2	Quantitative limits（ng/L）	RSD
SMZ	y=-0.0382725+0.00620518x	0.9987	4.72	0.057%
TC	y=-0.00652143+0.0024038x	0.9931	2381.30	0.043%

Text S1

Antibiotic testing methods and LC-MS parameters. In this study, an ultra-high performance liquid chromatography-tandem mass spectrometer (UHPLC-MS-MS) from ThermoFisher, USA was used for the quantitative determination of the target antibiotics. The column temperature was set at 25 ℃, the injection volume was 5 μL, the mobile phase A was 0.3% formic acid water, the mobile phase B was pure acetonitrile, the initial mobile phase ratio was A:B=95:5, and the mobile phase flow rate was 0.25 mL/min. The gradient elution was used for the separation of the two antibiotics one by one.The 2 target antibiotics were detected simultaneously, and the detection modes were both positive ion mode. The relevant settings of the mass spectrometer were as follows: the ion source was a thermoelectric spray ionization source (HESI), the spray voltage was 4000 V, the evaporation temperature was 40 ℃, the sheath gas pressure was 35 arb, the auxiliary gas pressure was 3 arb, and the capillary temperature was 350 ℃. The scan mode was SRM, the scan time was 0.1 s, and the scan width was 1.0 m/z. The linear ranges of the two target antibiotics were 5-500 μg/L, and the internal standard method was used, and the specific evaluation parameters of the detection method are shown in Table S3